JEAS

JOURNAL OF ENGINEERING AND APPLIED SCIENCES

Journal of Engineering and Applied Sciences, Volume 20, Number 1, June 2022, 709 - 720

Development of a remote sensing system for detection and classification of oil spills using laser fluorosensor

Oborkhale, L.I.[1]; Aina, E.A.[2]; and Odo, K.O.[3*]

[1,2,3]Electrical and Electronic Engineering Department, Michael Okpara University of Agriculture, Umudike, Abia State

[*]Corresponding author's E-mail: kayceebby@yahoo.co.uk

Abstract

This paper focuses on the development of a remote sensing system for detection and classification of oil spills using laser fluorosensor. The slow response and intervention by the oil spill monitoring team over the years in Nigeria is due to the fact that oil spills are often detected very late and also the difficulty in making decision on the type of instruments to be deployed during clean-up. Early detection of oil spills and quick interventions are key elements in reducing this menace caused by oil spills in our environment. In this research work, oil spills classification system based on laser fluorosensor spectra data was modeled and simulated. Artificial Neural Network (ANN) toolbox in Matlab/Simulink with MLP (multi-layer perceptron) based supervised architecture was used for the simulation. Using the data in form of 90-channel spectra as inputs, the ANN presents the analysis and estimation results of oil products and various background materials as outputs. The network was trained to understand numerous spectra data of laser fluorosensor for different oil spill products (light oil, medium oil, and heavy oil) and other backgrounds (water, sand and stone). The trained network was tested using data set to the network. A back propagation learning algorithm with an optimizer based on gradient descent method was used during the training of the network. It was found that the ANN with MLP based supervised architecture performed well when the number of neurons in hidden layers is the same and an average of 100% classification result was achieved. It was also found that Laser fluorosensor must be operated at wavelength between 302nm and 340nm to produce well- distinguished fluorescence spectra.

Keywords: Artificial neural network, Laser fluorosensor, Multi-layer perception, Oil spill, Remote sensor.

1. Introduction

A remote sensing system plays an important role in continuous detection and classification of oil spills on oceans. This has helped the emergency and monitoring team to take a quick and proactive action in order to reduce pollution caused by oil spills in our environment, (Bava *et al.*, 2002). Oil spill is one of the major sources of pollution to the sea which can be accidental or deliberate. Sea-based sources are discharges coming from ships through leakages, ship accident and tank washing residues. Also, fuel oil sludge, engine room wastes and foul bilge water produced by all type of ships also end up in the sea (Konstantinos, 2014). The location and spread of an oil spill over a large area, the thickness of the spilled oil, the distribution of an oil spill to estimate the quantity of spilled oil, and the classification of the oil type. All these information are necessary in order to estimate environmental damage, take appropriate response activities, and to assist in clean-up operations (Maya, *et al.*, 2014).

Remote sensing data are basically records of electromagnetic wave reflected and emitted from the objects/earth features under investigation. The proportions of energy reflected, absorbed and transmitted will vary for various earth features, counting on their material type and condition. These differences permit us to differentiate different features on a picture. Even within a given feature type, the proportion of energy which is reflected, absorbed and transmitted will vary at different wavelengths. These two basic characteristics of electromagnetic radiation enable us to identify and study an object/earth feature, or in other words, to apply remote sensing (Shefali, 2010). Laser

Fluorosensors have been seen recently to be most effective remote sensors as they can detect oil under the water surface and on various backgrounds including snow or ice (Brown *et al.*, 2014).

Remote sensing data are basically records of electromagnetic wave reflected and emitted from the objects/earth features under investigation. The proportions of energy reflected, absorbed and transmitted will vary for various earth features, counting on their material type and condition. These differences permit us to differentiate different features on a picture. Even within a given feature type, the proportion of energy which is reflected, absorbed and transmitted will vary at different wavelengths. These two basic characteristics of electromagnetic radiation enable us to identify and study an object/earth feature, or in other words, to apply remote sensing (Shefali, 2010). Electromagnetic radiation is a form of energy moving through a free space which exhibits wave and light properties. The wave can be described in terms of wavelength (λ), which is the distance of separation between adjacent wave peaks, or its frequency (f), which is the number of wave peaks passing fixed point out a given time. Sensing systems collect information through several portions of the electromagnetic spectrum. In remote sensing, it is most common to categorize electromagnetic waves by their wavelength location within the electromagnetic spectrum. Although names are generally assigned to regions of the spectrum for convenience, there's no clear-cut line between one nominal spectral region and therefore the next. Divisions of the spectrum have grown out of the varied methods for sensing each sort of radiation quite from inherent differences within the energy characteristics of varied wavelengths, (Shashank, 2014).

The slow response and intervention by the oil spill monitoring team over the years in Nigeria has led to death of many aquatic animals, reduction in the yielding level of farm lands, and reduction in the quality of natural water available for human being. Therefore, distinguishing oil spills from various backgrounds and classifying oil spills into different products will go a long way in addressing the problem of late detection of oil spills and the slow decision making on the instruments to be deployed during clean-up.
The portions of the spectrum commonly utilized in remote sensing are:

i. Gamma rays, (less than 0.01nm)
ii. x-rays (0.01-10nm)
iii. ultraviolet, it adjoins the blue end of the visible portion of the spectrum (250-350 nm)
iv. visible (400-750nm),
v. Infrared, which adjoins the red end of the visible region and is further divided into three portions: near IR (0.7 – 1.3 μm), mid IR (1.3- 3μm) and thermal IR (3-100 μm)
vi. Microwaves (1mm-1m).

Spectral responses measured by remote sensors over various features at various wavelengths often permit an assessment of the sort and/or condition of the features and are often mentioned, as spectral signatures. Spectral signatures enable us to distinguish snow from water, vegetation from soil and so on.

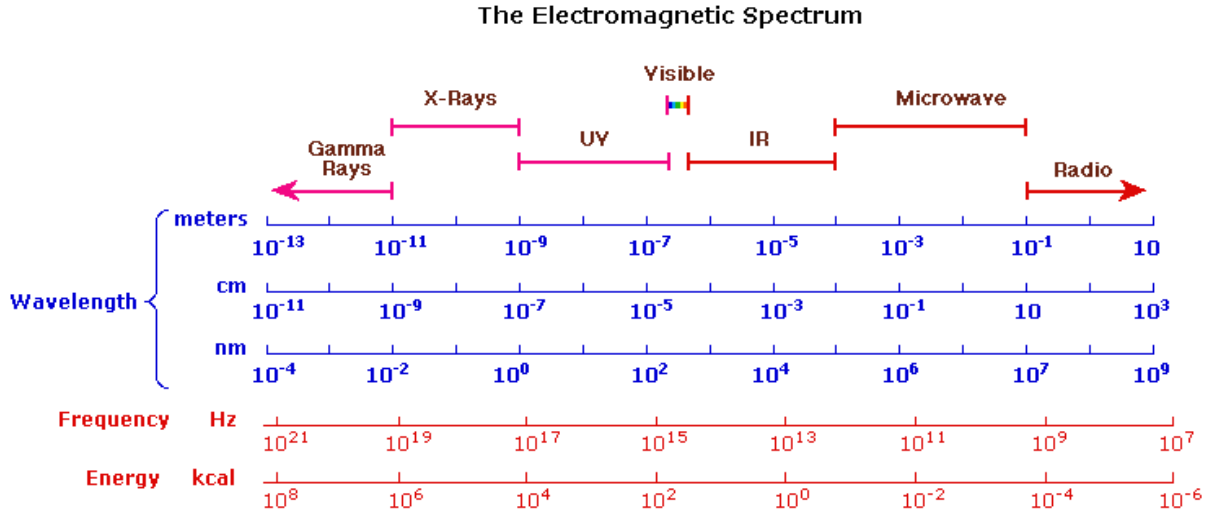


Figure 1: Region of Electromagnetic Spectrum (Mehta, 2011)

1.1 Literature Review

1.1.1 Related Works

Maya *et al.,* (2018) examined the characteristics and applications of different sensors. They observed that having a better understanding of the strengths and weaknesses of oil spill surveillance sensors will improve the operational use of these sensors for oil spill response and contingency planning. In the paper, Laser fluorosensors were found to be the most efficient sensors for oil spill detection and also operate in either the day or night. However, they recommended more research on how a laser fluorosensor can be correctly be used to classify oil spills. Davide *et al.***,** (2019) introduced multiple oil spill typologies and existing frameworks and methods used as best practices for facing out the menace of oil pollution were reviewed and discussed. Specific tools based on information and communication technologies were then presented, considering in particular those which can be used as integrated frameworks for the specific challenges of the environmental monitoring of smaller oil spills. However, the research work did not consider using information and communication technologies to detect oil spills.

Sudhir *et al.,* (2019) examined oil spills recognition by utilizing Sentinel-1 (SAR-C) imageries. The result of this paper demonstrated the significance of the VV polarization (measures the proportion of vertical transmitted waves which return vertically to the sensor) of the Sentinel-1 for recognizing oil-spills just as the diminished utility of the VH polarization (measures the part of the emitted waves which are polarized at the earth's surface and return vertically to the sensor) in this sole circumstance. However, the authors stated that the major limitation of SAR is false detection From all the literatures reviewed, it can be seen that none of the authors has used laser fluorosensor spectra data of different oil spill products and other backgrounds as a vector data to train a multi-layer Perceptron (MLP) network of an artificial neural network which is used to model and simulate an oil spills classification system that will distinguish oil spills from other backgrounds and also classify oil spill into different products in Matlab.

2.0 Materials and method

The materials required in this research work are Laser fluorosensor spectra data of different oil spill products and other backgrounds collected from national oil spill detection and response agency in Nigeria (NOSDRA), Multi-Layer Perceptron (MLP) Model of an Artificial Neural Network, MATLAB/SIMULINK R2015b software and HP window 10, 4GB Installed Memory, 64-bit operating system laptop.

2.1 Method

The laser fluorosensor spectra data was tabulated and analyzed with Microsoft excel. The oil spills classification system was first modeled using a Multi-Layer Perceptron (MLP) model of an Artificial Neural Network technique. Then a MLP network training flow chart/oil spill classification scheme was developed. The oil spills classification system was simulated using an Artificial Neural Network toolbox in Matlab/Simulink with MLP based supervised architecture. The simulated artificial neural network was trained to understand numerous spectra data of laser fluorosensor for different oil spill products (light oil, medium crude and heavy oil) and other backgrounds (water, sand and stone). A back propagation learning algorithm with an optimizer based on gradient descent method was used during the training of the network. The trained network was then used to distinguished oil spills from other backgrounds and also classify oil spills into different products. The performance, accuracy and precision of the trained network were evaluated by root mean square error, regression curve and ROC (Receiver Operating Characteristic) curve.

2.1.1 Artificial neural network model

The general model for an artificial neural network used in this research work as stated in (Aharkava *et al*., 2010) is given as

$$Y = g[(\sum_{i=1}^{n} x_i w_i) + b] \quad (1)$$

where

Y = Predicted Output

g = Activation function

x = Input signal

w = Weight

b = Bias

The activation function used is a sigmoid function as stated in (Gil *et al*., 2010) is given as

$$g(h) = \frac{1}{[1 + exp^{(-h)}]} \quad (2)$$

2.1.2 Multi-layer Perceptron (MLP) Model

The MLP model used in this research work has one input layer that receives external input, two hidden layers where transformation is taking place and one output layer which generates the classification results. Each neuron in the input and the hidden layers is connected to all neurons in the next layer by weighted connections. Each neuron n_j is associated with a weight vector $w_j \in R^n$.

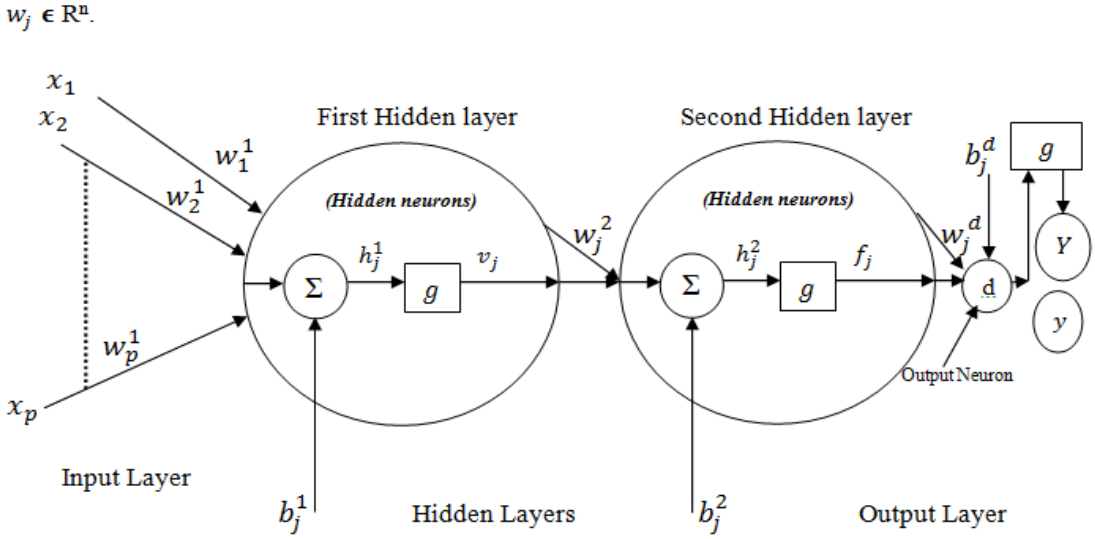


Figure 2: Multi-Layer Perceptron model with one input layer, two hidden layers and one output layer. (Gil *et al*., 2010)

x_i= Input sample
w_i^1= Connection weight of a neuron in the first hidden layer
h_j^1 = The weighted sum plus the bias b_j^1 to each neuron in the first hidden layer
w_j^2= Connection weight of a neuron in the second hidden layer
h_j^1 = The weighted sum plus the bias b_j^2 to each neuron in the second hidden layer
w_j^d= Connection weight of neuron d in the output layer
b_j^d = The bias for the neuron d in the output layer.
Σ = Transfer function
g = Activation function
Y = Predicted output
y = Actual output

Each neuron n_i in the first hidden layer receives an input vector $x_i \in R^n$. The net input vector h_i^1 to the neuron is given by

$$h_j^1 = \sum_{i=0}^{p} w_i^1 x_i + b_j^1 \quad (3)$$

The output v_j from the first hidden layer is calculated by using a sigmoid function

$$v_j = g(h_j^1) = \frac{1}{[1+\exp(-h_j^1)]} \quad (4)$$

Similarly, the net input vector h_j^2 to each neuron in the second hidden layer is given by

$$h_j^2 = \sum_{j=0}^{p} w_j^2 v_j + b_j^2 \quad (5)$$

The output f_j from the second hidden layer is calculated by using a sigmoid function

$$f_j = g(h_j^2) = \frac{1}{[1+\exp(-h_j^2)]} \quad (6)$$

Similarly output neuron *d* receives a net input of

$$m_{pd} = \sum_{j=0}^{p} w_j^d f_j \quad (7)$$

Here, w_j^d represents weight from the second hidden layer to the output neuron d. The neuron then outputs quantity expressed by relation

$$Y_{pd} = g(m_{pd}) = \frac{1}{[1+exp^{(-m_{pd})}]} \quad (8)$$

Since MLP is a supervised artificial neural network, that is, the network is presented with input samples as well as corresponding desired output, error function E is therefore minimized using Gradient descent optimizer through backward propagation algorithm is given as

$$E = \frac{1}{2}[\sum_{i=1}^{p}(y - Y)^2] \quad (9)$$

where y and Y are desired output and predicted output respectively. The error E is Mean Square Error (MSE). The square root of error E is Root Mean Square Error (RMSE). The weights are therefore adjusted to change the value of E in the direction of its negative gradient. The exact updating rules are calculated by applying derivatives and chain rule for the weights between the input layer and the output layer. The objective function given by equation 9 is a function of unknown weights w_j^1, w_j^2, and w_j^3. So, partial derivative functions with respect to weights was evaluated and then move weights in a direction down the slope, continuing until error function no longer decreases. Mathematically, this can be expressed by

$$\Delta w_j^d = \frac{-\eta \partial E}{\partial w_j^d} \quad (10)$$

Where η is the learning rate and simply scale step size.

From equation 8,

$$\frac{\partial Y}{\partial m_{pd}} = g'(m_{pd}) = Y(1 - Y) \quad (11)$$

From equation 7,

$$\frac{\partial m_{pd}}{\partial w_j^d} = f_j \quad (12)$$

Equation 11 was multiplied by equation 12 to get,

$$\frac{\partial Y}{\partial m_{pd}} * \frac{\partial m_{pd}}{\partial w_j^d} = \frac{\partial Y}{\partial w_j^d} = [Y(1 - Y] * f_j \quad (13)$$

Also from equation 9,

$$\frac{\partial E}{\partial Y} = (-1)y - Y \quad (14)$$

Using chain rule, equation 13 was multiplied by equation 14 to get,

$$\frac{\partial Y}{\partial w_j^d} * \frac{\partial E}{\partial Y} = \frac{\partial E}{\partial w_j^d} = [(-1)y - Y] * [Y(1 - Y]f_j \quad (15)$$

Substituting equation 15 back to equation 10, change in weights from the second hidden layer is given by

$$\Delta w_j^d = -\eta[(-1)y - Y]Y(1 - Y)f_j \quad (16)$$

Weights are updated as

$$w_j^d(t + 1) = w_j^d(t) + \Delta w_j^d \quad (17)$$

Therefore, MLP network is trained by following the processes below

a. Initialize the weights to small random values.
b. Choose an input vector and propagate it forward. This yields values for v_j, f_j and Y, the outputs from the first hidden layer and the second hidden layer and output layer respectively.
c. Compute mean square error
d. Update weights

Since the input layer, the hidden layers and the output layer are all vectors, then, matrices can be used to summarize all the equations. The artificial neural network designed in this thesis has six input signals, two hidden layers and six outputs. Each of the hidden layers has seven neurons which are arranged vertically.

3.0 Results and Discussion

The network was trained with an input data which is in form of matrix or vector as shown in Table 1. The network was first trained with two hidden layers and each of the hidden layers having seven neurons. Then the number of hidden layers and number of neurons in each hidden layer were varied and their respective effects on the network were observed.

Table 1: Laser fluorosensor wavelengths/corresponding relative intensities of all the substances

S/N	Laser Fluorosensor Wavelength (nm)	INPUT DATA MATRIX (90 X 6) Relative Intensities of the substance					
		Light Oil	Medium Crude	Water	Heavy Oil	Sand	Stone
1	301	152	56	82	78	81	66
2	302	188	72	98	99	102	87
3	303	196	85	122	147	144	124
4	304	232	106	145	188	186	148
5	305	256	158	184	193	202	163
6	306	333	170	200	200	247	170
7	307	310	170	340	200	257	170
8	308	324	170	345	600	274	170
9	309	324	1978	344	1200	305	170
10	310	345	5034	354	2200	320	170
11	311	372	4139	355	2600	329	190
12	312	418	2267	379	3490	345	206
13	313	454	1309	400	4009	361	219
14	314	523	1590	426	4264	359	231
15	315	699	1697	416	4166	366	270
16	316	817	1996	399	3999	365	309
17	317	962	2401	366	3666	372	312
18	318	1172	2669	379	3796	364	351
19	319	1761	3012	601	3501	409	366
20	320	2112	3113	989	3469	431	376
21	321	2660	3219	1211	3311	435	356
22	322	3232	3362	1513	3113	469	335
23	323	3961	3261	1819	2919	493	319
24	324	4689	3323	2162	2762	516	293
25	325	5565	3108	2461	2561	505	276
26	326	6395	3208	2823	2423	576	251
27	327	7371	3148	3210	2210	586	231
28	328	8130	3093	3699	1999	595	219
29	329	8878	2961	3969	1769	585	200
30	330	11173	2864	4161	1548	669	180
31	331	11314	2767	4293	1403	625	170
32	332	10931	2649	4161	1361	667	170
33	333	9594	2586	3964	1264	657	170
34	334	7690	2413	3867	1167	622	170

35	335	5411	2309	3549	1049	641	170
36	336	3313	2205	2999	986	646	170
37	337	1862	2101	2689	813	699	170
38	338	1058	1999	2409	709	676	170
39	339	636	1897	2255	605	686	170
40	340	436	1797	2001	501	654	170
41	341	288	1647	1899	499	647	170
42	342	265	1520	1697	397	623	170
43	343	246	1490	1247	297	592	170
44	344	241	1385	1020	247	564	170
45	345	245	1280	800	220	586	170
46	346	237	1180	689	190	594	170
47	347	238	1080	590	185	584	170
48	348	239	980	478	180	563	170
49	349	240	880	356	180	548	170
50	350	231	780	280	180	512	170
51	351	229	680	249	180	503	170
52	352	231	580	220	180	510	170
53	353	229	360	180	180	516	170
54	354	231	350	180	180	470	170
55	355	229	340	180	180	451	170
56	356	232	310	180	180	435	170
57	357	231	290	180	180	436	170
58	358	229	270	180	180	426	170
59	359	234	275	185	185	431	175
60	360	239	280	190	190	436	180
61	361	244	285	195	195	441	185
62	362	249	290	200	200	446	190
63	363	254	295	205	205	451	195
64	364	259	300	210	210	456	200
65	365	264	305	215	215	461	205
66	366	269	310	220	220	466	210
67	367	274	315	225	225	471	215
68	368	279	320	230	230	476	220
69	369	284	325	235	235	481	225
70	370	289	330	240	240	486	230
71	371	294	335	245	245	491	235
72	372	299	340	250	250	496	240
73	373	304	345	255	255	501	245
74	374	309	350	260	260	506	250
75	375	314	355	265	265	511	255
76	376	319	360	270	270	516	260
77	377	324	365	275	275	521	265

78	378	329	370	280	280	526	270
79	379	334	375	285	285	531	275
80	380	232	250	180	180	385	170
81	381	233	220	180	180	377	170
82	382	231	180	180	180	379	170
83	383	230	180	180	180	378	170
84	384	233	180	180	180	348	170
85	385	240	180	180	180	336	170
86	386	240	180	180	180	328	170
87	387	258	180	180	180	333	170
88	388	258	180	180	180	180	170
89	389	258	180	180	180	180	170
90	390	258	180	180	180	180	170

The relative intensities of all the substances were plotted against their respective wavelengths of the laser fluorosensor as tabulated in Table 1

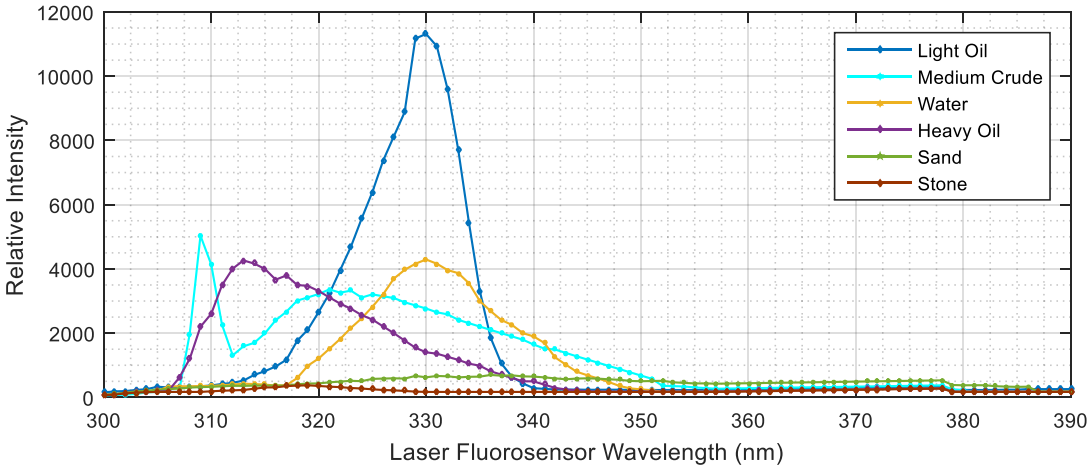


Figure 3: Fluorescence spectra of oil products and background materials

It was observed from figure 3 that the fluorescence spectra curves of all the substances (light oil, medium crude, heavy oil, water, sand and stone) can be well distinguished between 310nm and 340nm of laser fluorosensor wavelengths. It was also observed that the fluorescence spectra curve of light oil has highest amplitude follow by medium crude, water, heavy oil, sand and the stone spectra curve has the lowest amplitude.

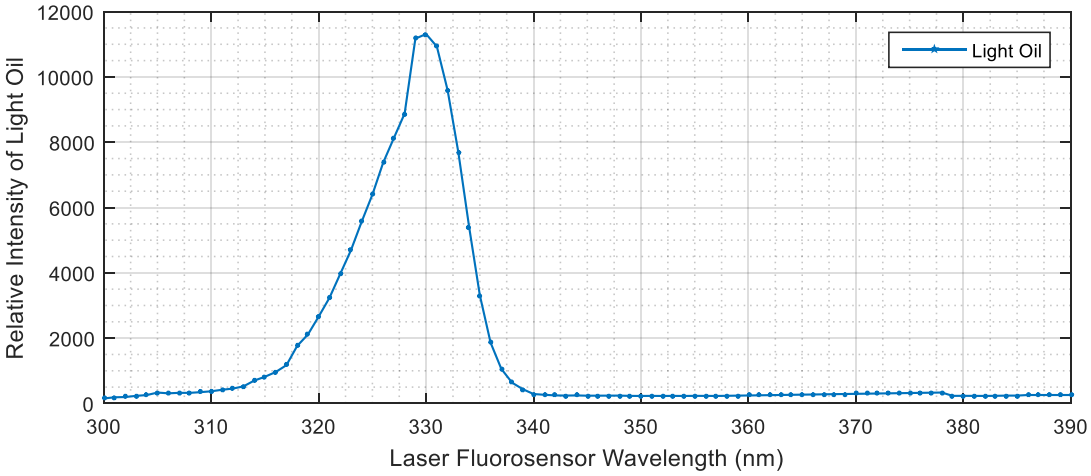


Figure 4: Fluorescence spectra of light oil

It was also observed that the fluorescence spectra curve of light oil attained maximum amplitude at 330 nm at relative intensity of 11,800 as shown in Figure 4.

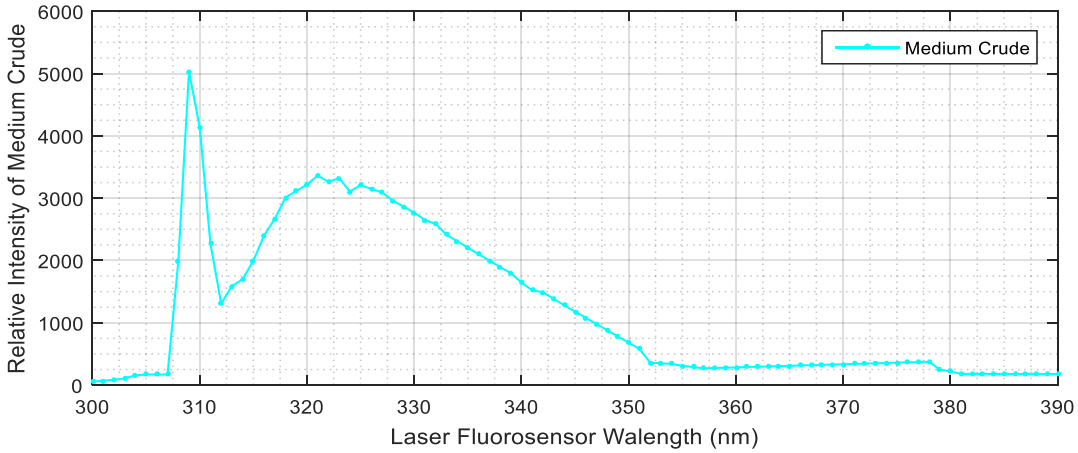


Figure 5: Fluorescence spectra of medium crude

The fluorescence spectra curve of medium crude attained maximum value at 309 nm at relative intensity of 5000 as shown in Figure 5.

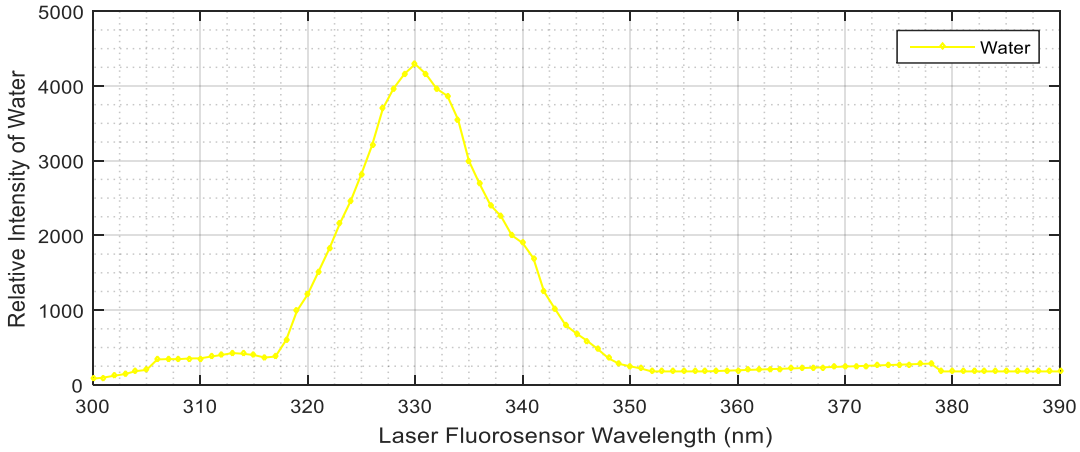


Figure 6: Fluorescence spectra of water

The fluorescence spectra curve of water attained maximum value at 330 nm at relative intensity of 4400 as shown in Figure 6.

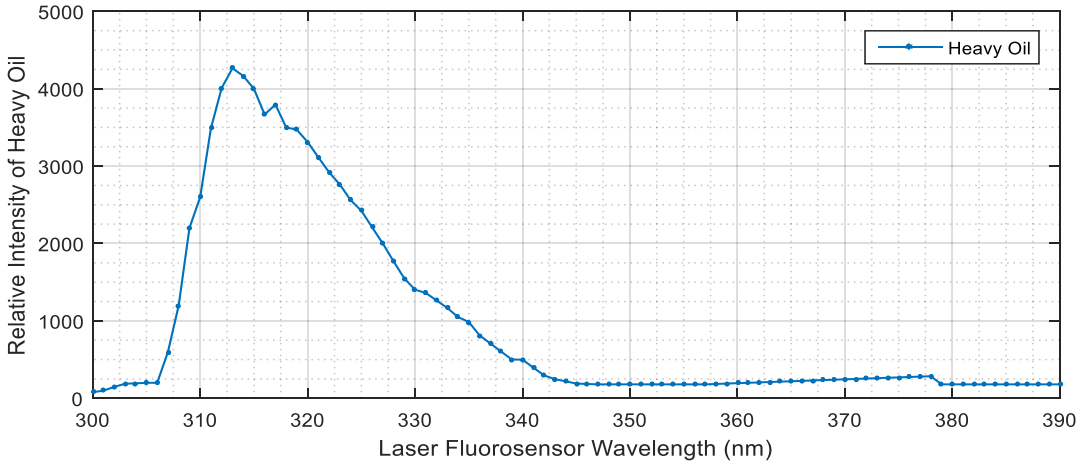


Figure 7: Fluorescence spectra of heavy oil

The fluorescence spectra curve of heavy oil attained maximum value at 314 nm at relative intensity of 4250 as shown in Figure 7.

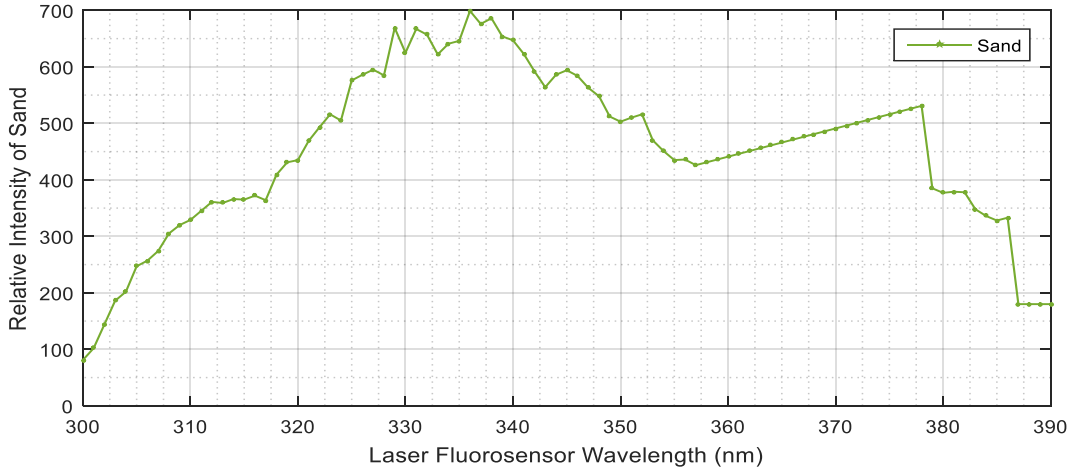


Figure 8: Fluorescence spectra of sand

The fluorescence spectra curve of sand attained maximum value at 337 nm at relative intensity of 700 as shown in Figure 8.

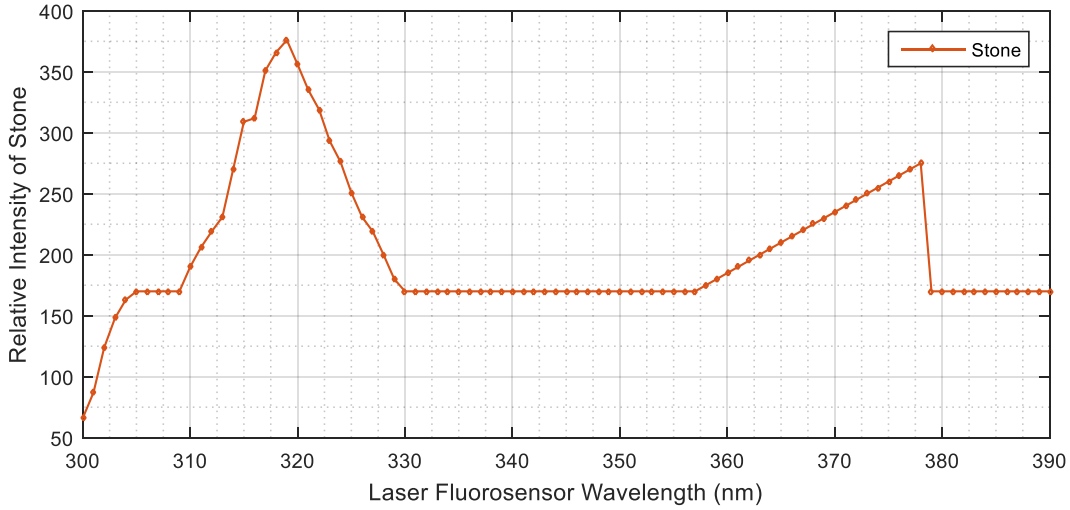


Figure 9: Fluorescence spectra of stone

The fluorescence spectra curve of stone attained maximum value at 319 nm at relative intensity of 375 as shown in figure 9. It is seen that laser fluorosensors can be operated at wavelength between 308 nm and 340 nm since the fluorescence spectra curves of all the substances can be well distinguished at these wavelengths.

4.0. Conclusion

The modelling of ANN with MLP based supervised architecture was simulated and trained with laser fluorosensor spectra data under different number of hidden layers and different number of neurons in hidden layers and the results were analysed using Matlab. MLP was found to be a very suitable tool for the simulation of oil spills classification system. The simulation results will be helpful in the hardware implementation of the system. It was found that the number of hidden layers as well as number of neurons in the hidden layers have a significant effect on the successful training of the network hence, the overall performance and accuracy of the network. From the research work, it was observed that laser fluorosensors can operate at wavelengths between 308 nm and 340 nm since the fluorescence spectra curves of all the substances can be well distinguished at these wavelengths.It was found that laser fluorosensors were the best among remote sensors in their usefulness for detecting and monitoring oil spills and most efficient sensors for oil spill detection since they can detect, classify oil on all surfaces and also operate in either the day or night.

5.0 Recommendation

The laser fluorosensor spectra data used in this research work is limited to six substances which are light oil, medium crude, heavy oil, water, sand and stones. It is therefore recommended that more substances should be added in future research to give the network more flexibility.

Acknowledgements

The support of National Oil Spill Detection and Response Agency in Nigeria (NOSDRA) is gratefully acknowledged for providing Laser fluorosensor spectra data of different oil spill products used for this research work.

References

Bava J., Tristan O., and Yasnikouski J. 2002. Earth observation applications through systems and instruments of high performance computer. *ASI/CONEA training course*, September-December, Matera, Italy, pp. 485-631

Bianchi F., Espeeseth M., and Borch N. 2020. "Large scale detection and categorization of oil spills from SAR images with deep learning. Remote sensor, 12, 2260.

Brown, C., Fingas M., Marois R., and Gamble R. 2014, Remote Sensing of Water-In-Oil Emulsions: Initial Laser Fluorosensor Studies. *Proceedings of the 27th Arctic and Marine Oil spill Program (AMOP) Technical Seminar*, Environment Canada, Ottawa, ON, Canada, pp. 295-306.

Carl E. B. and Merv F. (2018). A review of oil spill remote sensing. *Spill science Edmonton*, AB T6W 1J6, Canada, *18*(1):91.

Davide M., Gabriel P. and Marco T. 2019. Environmental Decision Support Systems for Monitoring small scale Oil Spills Pollution. *Institute of information science and technologies, national research council, via Moruzzi, 1-56124 Pisa (IT) Italy*, pp.1-17

Konstantinos N. 2014. Oil Spill detection by SAR Images: Dark formation Detection, feature Extraction and classification Algorithms. *Joint Research Centre (JRC)*, European Commission, Via Fermi 2749, 21027, Ispra (VA), Italy, 8(10):6642-6659

Maya N., Jason L. and Yang G. 2014. Advances in remote sensing for oil disaster management. *State of the Art Sensors Technology for Oil Spill Surveillance:* Department of Geomatics Engineering, University of Calgary T2N 1N4, Alberta, Canada, Western Washington University, Disaster Reduction and Emergency Planning, Huxley College of the Environment, 516 High Street, Bellingham, Washington 98225-9085, USA, 8(1):236-255

Mehta A. 2011. Introduction to the Electromagnetic Spectrum and Spectroscopy. *Analytical chemistry*. ACS Publications (United States), 772

Mohamed S., Reem S., Hadi A.K., Adel K., Ahmed S., Shady E., Ali M., Mohammed G. and Ayman E. 2021. "A deep-learning framework for the detection of oil spills from SAR data" Multidisciplinary Digital Publishing Institute (MDPI), https://doi/10.3390/s21072351, 21(7), 2351.

Shashank G. 2014. Remote Sensing: History, Principles and Types. https://www.biologydiscussion.com/plant-taxonomy/remote-sensing-history-principles-and-types/30587, pp.15

Shefali A. (2010). Principles of Remote Sensing. *Photogrammetric and Remote Sensing Division*, Indian Institute of Remote Sensing, Dehra Dun, pp.16

Sudhir K., Saikat B. and Shashanklele 2019. An assessment of oil spill detection using sentinel 1 SAR-C images. *Journal of Ocean Engineering and Science*, 5(2):116-135

Sung H., Hyung S., Moung J., Won J. and Myoung J. 2017. Oil spill detection from planetscope image to detect oil spills. *Journal of Coastal Research*, 90(1):251-260